CONDENSED MATTER PHYSICS

Tuning across the BCS-BEC crossover in the multiband superconductor $Fe_{1+y}Se_xTe_{1-x}$: An angle-resolved photoemission study

Shahar Rinott,[1] K. B. Chashka,[1] Amit Ribak,[1] Emile D. L. Rienks,[2,3] Amina Taleb-Ibrahimi,[4] Patrick Le Fevre,[4] François Bertran,[4] Mohit Randeria,[5] Amit Kanigel[1]*

The crossover from Bardeen-Cooper-Schrieffer (BCS) superconductivity to Bose-Einstein condensation (BEC) is difficult to realize in quantum materials because, unlike in ultracold atoms, one cannot tune the pairing interaction. We realize the BCS-BEC crossover in a nearly compensated semimetal, $Fe_{1+y}Se_xTe_{1-x}$, by tuning the Fermi energy ε_F via chemical doping, which permits us to systematically change Δ/ε_F from 0.16 to 0.50, where Δ is the superconducting (SC) gap. We use angle-resolved photoemission spectroscopy to measure the Fermi energy, the SC gap, and characteristic changes in the SC state electronic dispersion as the system evolves from a BCS to a BEC regime. Our results raise important questions about the crossover in multiband superconductors, which go beyond those addressed in the context of cold atoms.

INTRODUCTION

The Bardeen-Cooper-Schrieffer (BCS) to Bose-Einstein condensation (BEC) crossover (*1*) has emerged as a new paradigm for pairing and superfluidity in strongly interacting Fermi systems, which interpolates between two well-known limiting cases: BCS theory for fermions with a weak attractive interaction and a BEC of tightly bound bosonic pairs. This crossover has now been extensively investigated in ultracold Fermi gas experiments (*2*–*4*), where the strength of the attraction between Fermi atoms is tuned using a Feshbach resonance. This has led to a number of new insights (*5*–*7*) into the very strongly interacting unitary regime that lies in between the BCS and BEC limits. One of the key characteristics of the crossover regime is that the ratio of the pairing gap Δ to the bandwidth or Fermi energy ε_F is of order unity, as opposed to the BCS limit, where $\Delta/\varepsilon_F = 1$.

From this perspective, most superconducting (SC) materials, even strongly correlated systems such as the cuprates, are much closer to the BCS limit than in the crossover regime. A key obstacle to realizing the BCS-BEC crossover in quantum materials is that one does not have the ability to continuously tune the strength of the pairing interaction that controls Δ. We offer an alternative path to the realization of the BCS-BEC crossover: Instead of trying to change Δ, we tune ε_F by chemically doping carriers and drive the system through the BCS-BEC crossover.

We focus on the Fe-based superconductor $Fe_{1+y}Se_xTe_{1-x}$, which is a nearly compensated semimetal (*8*–*10*), and tune the Fermi energies of various pockets by changing the excess Fe concentration y. Using angle-resolved photoemission spectroscopy (ARPES), we systematically map out the evolution of the electronic excitation spectrum to demonstrate that we traverse the BCS-BEC crossover in the solid state. Our work raises fundamentally new questions about the crossover in a multiband superconductor, which go beyond the single-band physics explored in cold atoms.

RESULTS

Our main results are summarized in Fig. 1, where we show the ARPES intensity at 1 K, well below SC T_c, for a hole band near the Γ point of the Brillouin zone. The top three panels (Fig. 1, A to C) correspond to three samples in order of decreasing y, the amount of excess Fe. We deduce the following important results from these data.

(i) From the electronic dispersion far from the chemical potential, which is the same in the normal and SC states, we estimate ε_F, the unoccupied bandwidth for this hole pocket, and show that it systematically decreases with decreasing y.

(ii) We measure the SC energy gap Δ from the energy of the coherence peaks in the spectra, which correspond to the Bogoliubov quasiparticles. We find $\Delta = 3 \pm 0.5$ meV for all three samples. We conclude that the dimensionless measure of the pairing strength $\Delta/\varepsilon_F = 0.16$, 0.3, and 0.5 increases monotonically with decreasing y, exhibiting a crossover from a BCS to a BEC regime.

(iii) As Δ/ε_F increases, we see that the dispersion of the coherence peak changes from being BCS-like dispersion, with characteristic backbending near k_F, to the unusual BEC-like dispersion, with a minimum gap at $k = 0$. This can also be viewed as the shrinking of the "minimum gap locus" (*11*) from a contour enclosing a finite area in the large y BCS regime to a single point in the small y BEC regime, consistent with the prediction (*12*) of the crossover theory for multiband SCs (*13*, *14*). We show in Fig. 1 (D to F) the spectral function obtained from a simple model and describe below how it captures important features of the BCS-BEC crossover.

Our work builds on recent experimental progress in Fe(Se,Te). We have previously shown (*15*) that a small y sample had a tiny ε_F of a few millielectron volts and a large Δ/ε_F that places it well outside the weak coupling BCS limit. The small value of ε_F in $Fe_{1+y}Se_xTe_{1-x}$ has also been reported by Okazaki *et al.* (*16*), which focused on an unoccupied electron band just above ε_F. Small values of ε_F were also found in FeSe (*17*), together with the observation (*18*) of anomalously large SC fluctuation effects attributed to preformed pairs above T_c. The results presented here go beyond these earlier works in that we show how a systematic change in ε_F via doping permits us to tune across the BCS-BEC crossover.

Materials and transport data

Bulk FeSe has been intensively investigated. It exhibits nematic ordering without antiferromagnetic long-range order (in contrast to other Fe pnictides) (*19*) and becomes a $T_c = 65$ K superconductor in monolayer thin-film form on various substrates (*20*–*22*). Here, we focus on the

[1]Department of Physics, Technion–Israel Institute of Technology, 32000 Haifa, Israel. [2]Leibniz-Institut für Festkörper- und Werkstoffforschung Dresden, D-01171 Dresden, Germany. [3]Institut für Festkörperphysik, Technische Universität Dresden, D-01062 Dresden, Germany. [4]Synchrotron SOLEIL, Saint-Aubin, BP 48, F91192 Gif sur Yvette Cedex, France. [5]Department of Physics, Ohio State University, Columbus, OH 43210, USA. *Corresponding author. Email: amitk@physics.technion.ac.il

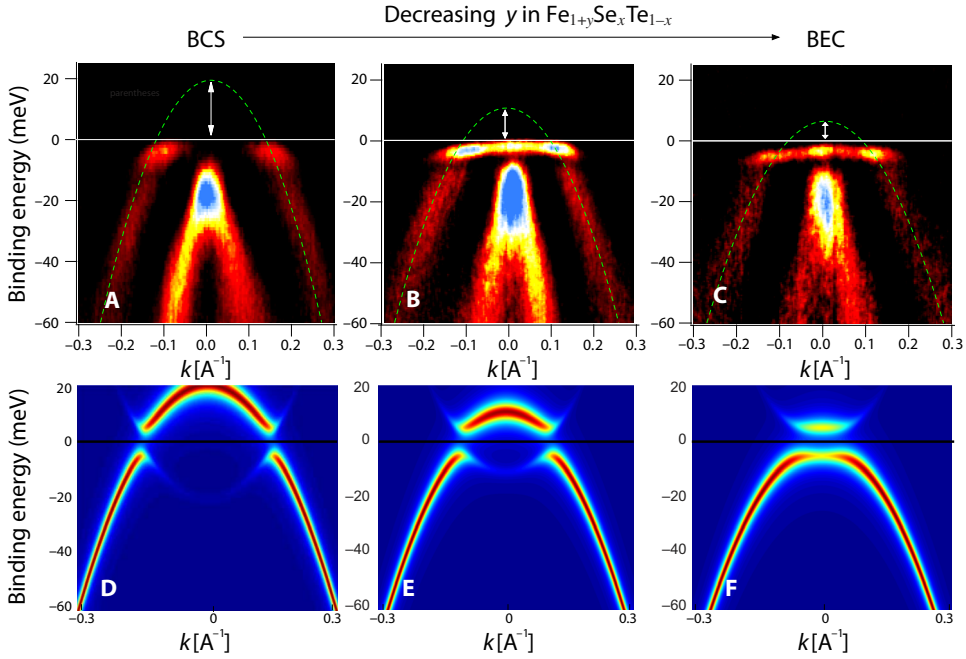

Fig. 1. SC state ARPES spectra. (**A** to **C**) ARPES spectra for three $Fe_{1+y}Se_xTe_{1-x}$ samples in order of decreasing *y* (excess Fe) from left to right. The spectra are normalized using the intensity from high-order photons, and a constant background is removed. The spectra are sharpened by adding a small part of their second derivative to the original data. The green dashed line is the best fit to the data using a simple parabolic dispersion. (**D** to **F**) Spectral functions, calculated using the model and parameters described in the text, to describe the BCS-BEC crossover seen in the data in the top panels.

lower T_c bulk material Fe(Se,Te), which is nevertheless the most strongly correlated in this family with the largest Δ/ε_F ratios, as we show below.

A series of $Fe_{1+y}Se_xTe_{1-x}$ samples were prepared using the modified Bridgman method. We chose to fix $x = 0.4$ near the maximum $T_c \simeq 15$ K for *y* near zero. The composition *x* was measured by energy-dispersive x-ray (EDX) analysis. Recently, it was shown that, by annealing in oxygen, it is possible to reduce *y*, the amount of excess Fe (*23*–*27*). Attempts, made by us and other groups, to quantify *y* using standard techniques, such as EDX, x-ray diffraction, and inductively coupled plasma, have resulted in inconclusive results. It seems that the only reliable way to measure *y* is to simply count the number of excess Fe atoms using a scanning tunneling microscope (*27*). We note that a quantitative determination of *y* in our samples is not essential to our study, because we will focus on the resulting systematic changes in ε_F measured by ARPES, as shown below.

The result of reducing *y* is an increase in T_c and a change in the resistivity as a function of temperature. In addition, it was found that the annealing process changes the sign of the Hall resistivity at low temperatures. The samples shown in Fig. 1 are ordered from large value of *y* (BCS) to small value of *y* (BEC) based on their T_c and resistivity curves.

In Fig. 2 (B and C), we show dc transport data for two samples: The small *y* sample (red curve) has an SC $T_c = 14$ K, whereas the large *y* sample (blue curve) has $T_c = 12$ K. Using a SQUID magnetometer, we verified that all the crystals used have a full SC shielding volume fraction. Note that the entire *T* dependence of the resistivity in Fig. 2B is different for the two samples.

The Hall resistance R_H for the same samples shown in Fig. 2C also depends strongly on *y*. At low temperatures, the small *y* sample has a negative R_H, whereas the large *y* sample has a positive R_H, in agreement with previous reports (*23*). A quantitative analysis of the Hall data is difficult in view of the multiple bands involved.

Electronic structure

To understand our ARPES results, it is useful to first look at the schematic of the band structure of Fe(Se,Te) (see Fig. 2A). In bulk FeSe, Fe^{2+} is in a $3d^6$ configuration. With an even number of electrons per unit cell, FeSe is a compensated semimetal, which should be unaffected by the isovalent substitution of Se by Te. Changing *y* in $Fe_{1+y}Se_xTe_{1-x}$ alters the balance between electrons and holes in what was an almost perfectly compensated semimetal (*23*–*25*, *28*).

In Fig. 2A, we show the three hole bands α_i [$i = 1$, 2, and 3 in the notation of Tamai *et al.* (*29*)] near the Γ point and two electron bands (due to zone folding) near the *M* point of the Brillouin zone. The red curves in Fig. 2A denote the bands for the small *y* sample, whereas the blue curves correspond to the large *y* sample. The main focus of our attention in this paper is the light-hole band α_2, but we will also discuss some features of the heavy-hole band α_3 (which remains at or just below the chemical potential) and the electron band near *M*. The α_1 band is always well below the chemical potential. A key observation below is that changing excess Fe does not just shift the chemical potential in a rigid band structure. Some bands shift in energy, whereas others do not. In addition, changing *y* leads to mass renormalizations.

ARPES data for electron and hole bands

In Fig. 3 (A to D), we compare ARPES data for the electron pocket around the *M* point for the two samples in Fig. 2. We show the ARPES intensity in Fig. 2A and the momentum distribution curves (MDCs) in Fig. 2C for the small *y* sample, whereas Fig. 2 (B and D) shows the corresponding data for the large *y* sample. The green lines in Fig. 2

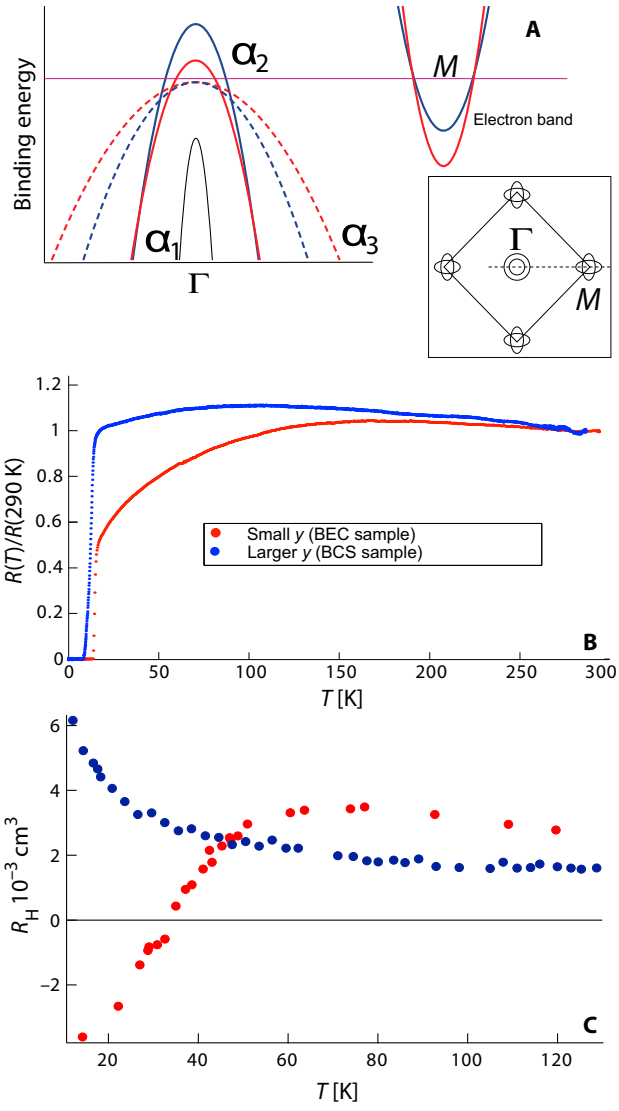

Fig. 2. Schematic of electronic structure and transport data for $Fe_{1+y}Se_xTe_{1-x}$ samples with different amounts of excess Fe *y*. In all panels, the red and blue curves correspond to the small and large *y* samples, respectively. (**A**) Schematic band structure and the effect of *y* on various bands (see text for details). (**B**) Resistivity (*R*) as a function of temperature (*T*). The small *y* sample has an SC T_c = 14 K, whereas the large *y* sample has T_c = 12 K. (**C**) Hall resistance R_H of the same two samples. R_H of the small *y* sample changes sign at around 40 K, whereas that for the large *y* sample is always positive.

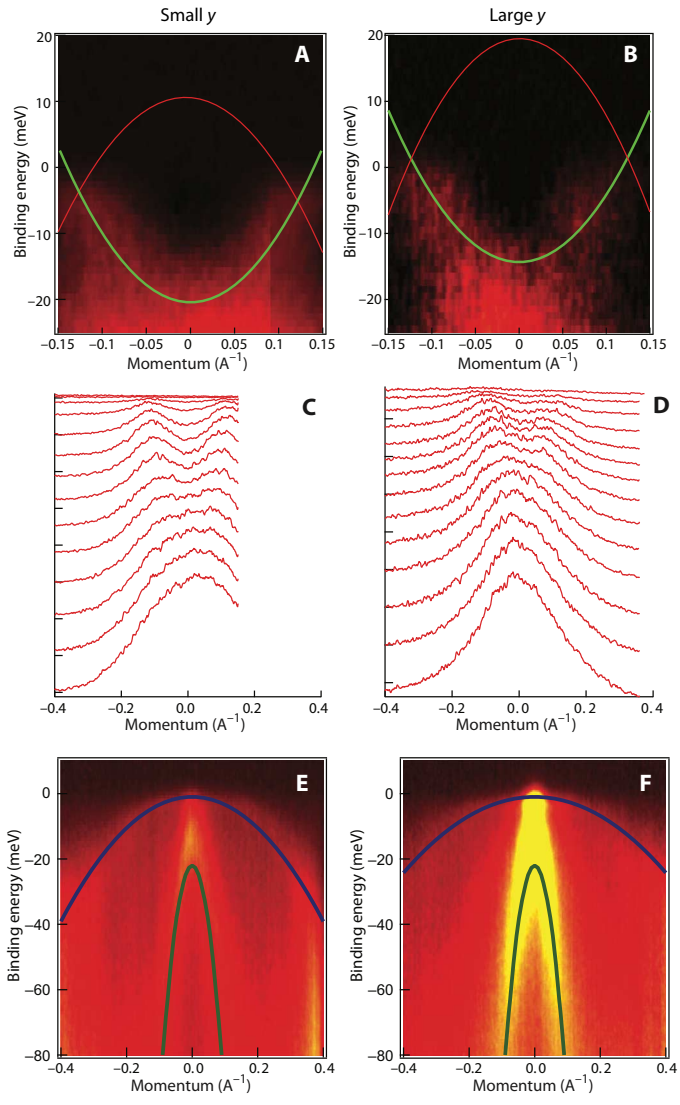

Fig. 3. ARPES data showing the effect of *y* on the band structure. (**A** and **B**) ARPES spectra around the *M* point for two samples with small and large amounts of excess Fe, respectively. A shallow electron pocket can be seen, whose occupied bandwidth decreases with excess Fe. (**C** and **D**) The green lines are best fits using a simple parabolic model to the MDCs. The red lines represent the α_2 dispersion for the same samples. (**E** and **F**) ARPES spectra of the same two samples around the Γ point using vertically polarized 22-eV light. In this polarization, α_1 and α_3 can be seen. The blue curves represent the dispersion of α_3, and the green lines represent that of α_1.

(A and B) represent the best parabolic fits to the MDC maxima shown in Fig. 2 (C and D, respectively). We see that the Fermi energy (occupied bandwidth for the electron band) changed from 20 meV (small *y* sample) to 14 meV (large *y* sample), whereas the effective mass is 3.7 m_e for both. We can compare the change in the electron pocket dispersion (green lines in Fig. 2, A and B), with excess Fe content *y*, to the corresponding α_2 dispersion (shown as red curves). The latter is obtained from the measured α_2 MDC peaks around the Γ point (see Fig. 4). With increasing *y*, as the electron dispersion moves up in energy near the *M* point, so does the hole dispersion near Γ. This is qualitatively consistent with the increasing hole-like character of the Hall data in Fig. 2, with increasing *y*. We note that, in the ARPES geometry that we use (vertical polarization along the Γ – *M* direction), we observe only one of the electron pockets, and we do not observe any coherence peaks in the SC state spectra.

In contrast to the electron and α_2 hole bands, we do not find any significant shift in α_1 and α_3 bands as the excess Fe is changed. In Fig. 3 (E and F), we show the ARPES intensities for the small *y* (E) and large *y* (F) samples measured along a cut going through the Γ point, using a vertically polarized light. In this polarization, only the α_1 and α_3 bands can be seen (and not α_2). For all the samples that we have measured, the top of the α_1 band is at 22 ± 2 meV, that is, deep on the occupied side, in agreement with Lubashevsky *et al.* (*15*), Tamai *et al.* (*29*), and Miao *et al.* (*30*).

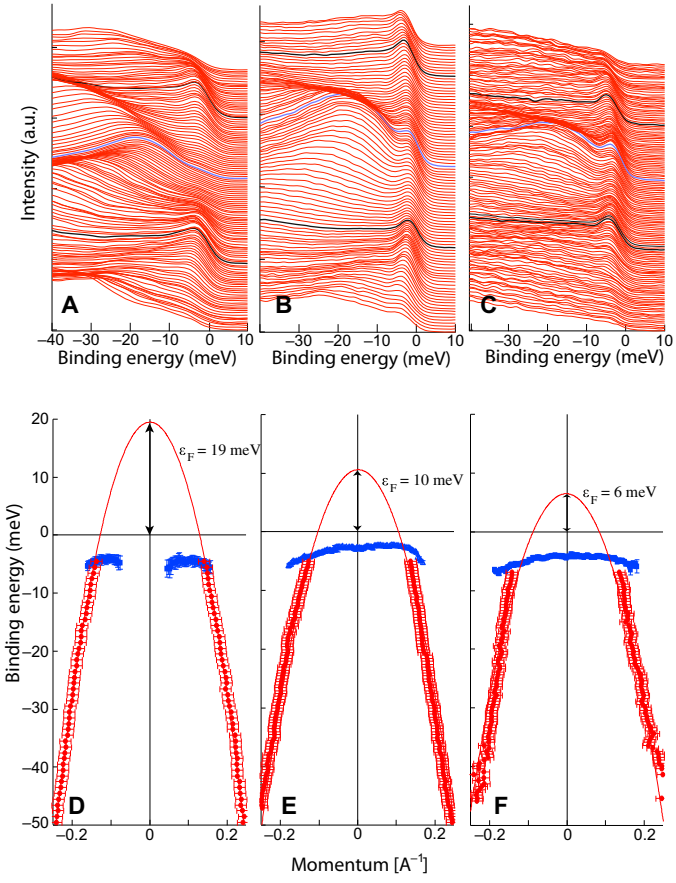

Fig. 4. Coherence peak dispersion in the SC state. (**A** to **C**) EDCs of the same three samples shown in Fig. 1 (A to C), measured at 1 K using horizontally polarized 22-eV photons. The blue line represents the EDC at the Γ point, and the black lines are the EDC at k_F. a.u., arbitrary units. (**D** to **F**) The blue dots represent the dispersion of the EDC coherence peaks extracted from (A) to (C), respectively. The red dots represent MDC peak positions for binding energies between −5 and −50 meV. The red lines are fits to the latter using a simple parabolic model.

We find that the α_3 hole band always has a rather low spectral weight. Nevertheless, we see that the unoccupied bandwidth is very small ($\varepsilon_F = -1 \pm 2$ meV) and does not change with y. Whether α_3 creates a hole pocket or not is not clear (*28*, *30*), although in FeSe α_3 is deep below the chemical potential (*31*).

The effective mass does change with excess Fe from 26 m_e for the small y sample to 16 m_e for the large y sample. Effective mass changes of the α_3 band were reported also in studies of the effect of Se-Te substitution on the band structure in $Fe_{1+y}Se_xTe_{1-x}$ (*32*).

ARPES evidence for BCS-BEC crossover

We finally describe the central results of this paper for the α_2 hole band (highlighted in Fig. 1). We show in Fig. 4 (A to C) the energy distribution curves (EDCs) for the three samples in Fig. 1 (A to C, respectively). The large y sample in Fig. 4A and the small y sample in Fig. 4B are the same ones for which we presented transport data above. The sample in Fig. 4C has the smallest value of y, the smallest amount of excess Fe, and a T_c = 14.5 K. The data in Figs. 1 and 4 were obtained using linearly polarized 22-eV photons at a temperature of 1 K (well below the SC T_c's of the samples) using a horizontal light polarization (*33*), in which only the α_2 and α_1 bands are visible.

To understand the effect of excess Fe on ε_F (the unoccupied bandwidth of the α_2 band), we analyze MDCs away from the low-energy region with the SC gap. The MDC peak positions from −5 to −50 meV are shown as red dots in Fig. 4 (D to F), with the three panels corresponding to the data in Fig. 1 (A to C, respectively). We note that the MDC peaks are the same, within our resolution, below and above T_c. Parabolic fits to the MDC peak dispersion are shown as red curves in Fig. 4 (D to F) and lead to ε_F estimates of 19, 10, and 6 meV for the three samples in order of decreasing y. The uncertainty in ε_F obtained from the fit (95% confidence bounds) was lower than 1.5 meV for all samples.

We determine the SC energy gap from the EDC peaks in Fig. 4 (A to C), which correspond to the coherent Bogoliubov quasiparticles in the spectral function below T_c. The dispersion of the EDC coherence peaks is shown as blue dots in Fig. 4 (D to F). Let us denote the experimentally determined Bogoliubov dispersion by $E(\mathbf{k})$. The SC gap Δ is given by the minimum of $|E(\mathbf{k})|$ along a $\mathbf{k}$-space cut perpendicular to the normal-state Fermi surface (here, a radial cut through Γ).

The SC gap for all three samples is Δ =3 ± 0.5 meV, in agreement with Lubashevsky *et al.* (*15*) and Miao *et al.* (*30*). We thus find Δ/ε_F = 0.16 (large y), 0.3 (small y), and 0.5 (smallest y). Thus, the important dimensionless ratio Δ/ε_F, which characterizes the pairing strength, increases monotonically with decreasing excess Fe, going from the BCS regime at large y to the BEC regime at small y.

Another important evidence for the BCS-BEC crossover comes from the characteristic change in the coherence peak dispersion. In the BCS regime, we expect a bending back of $E(\mathbf{k})$ for $k \approx k_F$, whereas in the BEC regime, the dispersion is qualitatively different with a minimum gap at $\mathbf{k} = 0$ (see the Supplementary Materials). This evolution is evident in both the raw ARPES data of Fig. 1 and the EDC peak dispersion in Fig. 4 (blue dots).

We can understand this better from the Bogoliubov dispersion $E(\mathbf{k}) = \sqrt{(\varepsilon_k - \tilde{\mu})^2 + \Delta^2}$, where $\varepsilon_k = \hbar^2 k^2/2m^*$, $\tilde{\mu}$ is a renormalized chemical potential, and Δ is the SC gap, which is assumed to be k-independent for simplicity. Exact numerical calculations (*34*) have shown that this form of the dispersion, well known from the mean-field theory, is accurate across the BCS-BEC crossover, provided one allows for renormalization of m^* and $\tilde{\mu}$ due to interaction effects. In the weak coupling BCS limit, $\tilde{\mu} = \varepsilon_F$, and the dispersion shows back-bending at k_F. More generally, in the BCS regime, where $\tilde{\mu} > 0$, E_k exhibits back-bending at $k^* = (2m^*\tilde{\mu})^{1/2}$. As one goes through the crossover, k^* decreases, which can also be described as the shrinking of the minimum gap locus (*11*). In the BEC regime, when $\tilde{\mu} < 0$, the locus has shrunk to a single point so that the dispersion has a minimum gap at $\mathbf{k} = 0$.

We use the BCS-inspired spectral function $A(k, \omega) = u_k^2\delta(\omega - E_k) + v_k^2\delta(\omega + E_k)$, with broadened delta functions, as a simple way to model our ARPES data (see the Supplementary Materials for details). In Fig. 1 (D to F), we plot $A(k, \omega)$ without the Fermi function that cuts off the ARPES intensity for unoccupied states at positive energies. We choose ε_F = 20, 10, and 2.5 meV in Fig. 1 (D, E, and F, respectively), with a fixed Δ = 5 meV. We adjust the chemical potential using $\tilde{\mu} = \varepsilon_F - \Delta^2/4\varepsilon_F$, the mean-field result for the two-dimensional BCS-BEC crossover (*35*). We see from Fig. 1 (D to F) that this simple model captures the evolution of SC state dispersion in the ARPES data. This analysis also gives insight into the ARPES spectral weight, which is controlled by the momentum distribution v_k^2. On the BCS side of the crossover, low-energy coherence peaks have significant spectral weight only near $k \approx k_F$, whereas on the BEC side, there is significant spectral weight in a large momentum range around $k = 0$. The fact that we focus on a hole band,

as opposed to an electron band, makes it much easier to observe the BEC-like regime using ARPES (see the Supplementary Materials).

DISCUSSION

Our main results are summarized in the Introduction, and we conclude with a discussion of the interesting open questions about the BCS-BEC crossover in multiband superconductors raised by our work. In contrast to the extensive theoretical literature (*5*–*7*) on the BCS-BEC crossover in single-band systems, motivated in large part by ultracold atom experiments, the crossover theory for multiband systems, especially nearly compensated semimetals, is much less developed [see, however, Lee Loh *et al.* (*12*), Leggett (*1*), and Chubukov *et al.* (*14*)].

We note that the evolution of the minimum gap locus from a contour in the BCS regime to a point in **k** space is a general consequence of the BCS-BEC crossover even in a multiband system (*12*). This also points to the interesting possibility that the crossover can be band-selective, namely, the pairing could be in a BEC regime on one band while in the BCS regime on another. This could well be the case for $Fe_{1+y}Se_{0.4}Te_{0.6}$, where we focused only on the crossover in the α_2 band. We found that, as the Fermi energy of the α_2 hole band near Γ is reduced, that on the electron band near M is increased. However, in the polarization geometry used, we do not see any SC state coherence peaks on the electron band, and new experiments are needed to see how the SC gap on that band changes with excess Fe.

The SC state BCS-BEC crossover reported in this paper raises several vital questions about the normal state. Do preformed pairs exist above T_c in Fe(Se,Te)? Is there a pairing pseudogap above T_c? We conclude with a discussion of the significance and implications of these issues.

A normal-state pseudogap was first observed in the underdoped high T_c superconductors, with ARPES playing a key role. We now understand that the cuprate pseudogap (*36*) has many facets, including the proximity to the Mott insulator, short-range singlet correlations, charge density wave fluctuations, and preformed pairing. In contrast, the pseudogap in the single-band BCS-BEC crossover originates from pairing. The normal state thus evolves from a Fermi liquid in the BCS limit to a normal Bose liquid in the BEC limit via the appearance of a pairing pseudogap in the crossover regime, as predicted early on (*37*). This pseudogap has been observed in the ultracold Fermi gases using a spectroscopic technique (*4*) analogous to ARPES.

For a multiband superconductor, such as Fe(Se,Te), the question is more complex than in the one-band case. Although the gaps, Fermi energies, and dispersions can be examined separately on each band by ARPES, there are fundamental properties of superconductors, such as the transition temperature T_c and the superfluid density ρ_s, that depend on all the bands and their mutual coherence. An understanding of how ρ_s and T_c evolve with Fe doping would shed light on the important questions of SC fluctuations and pseudogap above T_c. We note that recent diamagnetism experiments (*17*) on FeSe provide evidence for a large SC fluctuation regime above T_c. To date, however, there is no spectroscopic evidence for, or against, a pseudogap above T_c. This key question deserves further investigation.

MATERIALS AND METHODS

High-quality single crystals of $Fe_{1+y}Se_xTe_{1-x}$ were grown using the modified Bridgman method. The stoichiometric amounts of high-purity Fe, Se, and Te powders were grinded, mixed, and sealed in a fused silica ampoule. The ampoule was evacuated to a vacuum better than 10^{-5} torr, and the mixture was reacted at 750°C for 72 hours. The resulting sinter was then regrinded and put in a double-wall ampoule that was again evacuated to a vacuum better than 10^{-5} torr.

The ampoule was placed in a two-zone furnace with a gradient of 5°C/cm and slowly cooled from 1040° to 600°C at a rate of 2°C/hour, followed by a faster cooldown to 360°C for 24 hours. The resulting boule contained single crystals that could be separated mechanically. To change the amount of excess Fe, we annealed the crystals for 48 hours in ampoules that were evacuated and then filled them with different pressures of oxygen.

Transport measurements were performed using a homebuilt setup based on an Oxford Teslatron system. The resistivity and Hall resistance were measured using the van der Pauw method between room temperature and 2 K.

High-resolution ARPES measurements were performed at the UE112_PGM-2b-1^3 beamline at BESSY (Berlin, Germany) and at the CASSIOPÉE Beamline at SOLEIL (Saint-Aubin, France) using a photon energy of 22 eV. The samples were cleaved in vacuum better than 5×10^{-11} torr at base temperature and measured for not more than 6 hours. The base temperature at BESSY was 1 K and at SOLEIL was 7 K. The energy resolution was 4 meV in both beamlines.

SUPPLEMENTARY MATERIALS

Supplementary material for this article is available at http://advances.sciencemag.org/cgi/content/full/3/4/e1602372/DC1

Comparison between superconducting and normal state ARPES data

Modeling the spectral function

fig. S1. ARPES spectra above and below T_c.

fig. S2. Bogoliubov dispersion from BCS to BEC.

References (*38*, *39*)

REFERENCE AND NOTES

1. A. J. Leggett, Diatomic molecules and cooper pairs, in *Modern Trends in the Theory of Condensed Matter. Proceedings of the XVIth Karpacz Winter School of Theoretical Physics, Karpacz, Poland* (Springer-Verlag, 1980), pp. 13–27.
2. W. Ketterle, M. W. Zwierlein, Making, probing and understanding ultracold Fermi gases, in *Ultracold Fermi Gases, Proceedings of the International School of Physics "Enrico Fermi", Course CLXIV, Varenna, 20–30 June 2006*, M. Inguscio, W. Ketterle, C. Salomon, Eds. (IOS Press, 2008).
3. J. T. Stewart, J. P. Gaebler, D. S. Jin, Using photoemission spectroscopy to probe a strongly interacting Fermi gas. *Nature* **454**, 744–747 (2008).
4. J. P. Gaebler, J. T. Stewart, T. E. Drake, D. S. Jin, A. Perali, P. Pieri, G. C. Strinati, Observation of pseudogap behaviour in a strongly interacting Fermi gas. *Nat. Phys.* **6**, 569–573 (2010).
5. W. Zwerger, *The BCS-BEC Crossover and the Unitary Fermi Gas* (Springer, 2011).
6. M. Randeria, E. Taylor, Crossover from Bardeen-Cooper-Schrieffer to Bose-Einstein condensation and the unitary Fermi gas. *Annu. Rev. Condens. Matter. Phys.* **5**, 209–232 (2014).
7. Q. Chen, J. Stajic, S. Tan, K. Levin, BCS–BEC crossover: From high temperature superconductors to ultracold superfluids. *Phy. Rep.* **412**, 1–88 (2005).
8. K.-W. Yeh, T.-W. Huang, Y.-l. Huang, T.-K. Chen, F.-C. Hsu, P. M. Wu, Y.-C. Lee, Y.-Y. Chu, C.-L. Chen, J.-Y. Luo, D.-C. Yan, M.-K. Wu, Tellurium substitution effect on superconductivity of the α-phase iron selenide. *Europhys. Lett.* **84**, 37002 (2008).
9. Y. Xia, D. Qian, L. Wray, D. Hsieh, G. F. Chen, J. L. Luo, N. L. Wang, M. Z. Hasan, Fermi surface topology and low-lying quasiparticle dynamics of parent $Fe_{1+x}Te/Se$ superconductor. *Phys. Rev. Lett.* **103**, 037002 (2009).
10. I. Pallecchi, G. Lamura, M. Tropeano, M. Putti, R. Viennois, E. Giannini, D. Van der Marel, Seebeck effect in $Fe_{1+x}Te_{1-y}Se_y$ single crystals. *Phys. Rev. B* **80**, 214511 (2009).
11. R. Sensarma, M. Randeria, N. Trivedi, Can one determine the underlying Fermi surface in the superconducting state of strongly correlated systems? *Phys. Rev. Lett.* **98**, 027004 (2007).
12. Y. Lee Loh, M. Randeria, N. Trivedi, C.-C. Chang, R. Scalettar, Superconductor-insulator transition and Fermi-Bose crossovers. *Phys. Rev. X* **6**, 021029 (2016).
13. A. Guidini, A. Perali, Band-edge BCS-BEC crossover in a two-band superconductor: Physical properties and detection parameters. *Supercond. Sci. Technol.* **27**, 124002 (2014).

14. A. V. Chubukov, I. Eremin, D. V. Efremov, Superconductivity versus bound-state formation in a two-band superconductor with small Fermi energy: Applications to Fe pnictides/chalcogenides and doped $SrTiO_3$. *Phys. Rev. B* **93**, 174516 (2016).
15. Y. Lubashevsky, E. Lahoud, K. Chashka, D. Podolsky, A. Kanigel, Shallow pockets and very strong coupling superconductivity in $FeSe_xTe_{1-x}$. *Nat. Phys.* **8**, 309–312 (2012).
16. K. Okazaki, Y. Ito, Y. Ota, Y. Kotani, T. Shimojima, T. Kiss, S. Watanabe, C.-T. Chen, S. Niitaka, T. Hanaguri, H. Takagi, A. Chainani, S. Shin, Superconductivity in an electron band just above the Fermi level: Possible route to BCS-BEC superconductivity. *Sci. Rep.* **4**, 4109 (2014).
17. S. Kasahara, T. Watashige, T. Hanaguri, Y. Kohsaka, T. Yamashita, Y. Shimoyama, Y. Mizukami, R. Endo, H. Ikeda, K. Aoyama, T. Terashima, S. Uji, T. Wolf, H. von Lohneysen, T. Shibauchi, Y. Matsuda, Field-induced superconducting phase of FeSe in the BCS-BEC cross-over. *Proc. Natl. Acad. Sci. U.S.A.* **111**, 16309–16313 (2014).
18. S. Kasahara, T. Yamashita, A. Shi, R. Kobayashi, Y. Shimoyama, T. Watashige, K. Ishida, T. Terashima, T. Wolf, F. Hardy, C. Meingast, H. v. Löhneysen, A. Levchenko, T. Shibauchi, Y. Matsuda, Giant superconducting fluctuations in the compensated semimetal FeSe at the BCS-BEC crossover. *Nat. Commun.* **7**, 12843 (2016).
19. S. Medvedev, T. M. McQueen, I. A. Troyan, T. Palasyuk, M. I. Eremets, R. J. Cava, S. Naghavi, F. Casper, V. Ksenofontov, G. Wortmann, C. Felser, Electronic and magnetic phase diagram of β-$Fe_{1.01}Se$ with superconductivity at 36.7 k under pressure. *Nat. Mater.* **8**, 630–633 (2009).
20. Q.-Y. Wang, L. Zhi, Z. Wen-Hao, Z. Zuo-Cheng, Z. Jin-Song, L. Wei, D. Hao, O. Yun-Bo, P. Deng, C. Kai, W. Jing, S. Can-Li, K. He, J. Jin-Feng, J. Shuai-Hua, Y.-Y. Wang, L.-L. Wang, C. Xi, X.-C. Ma, Q.-K. Xue, Interface-induced high-temperature superconductivity in single unit-cell FeSe films on $SrTiO_3$. *Chinese Phys. Lett.* **29**, 037402 (2012).
21. R. Peng, H. C. Xu, S. Y. Tan, H. Y. Cao, M. Xia, X. P. Shen, Z. C. Huang, C. H. P. Wen, Q. Song, T. Zhang, B. P. Xie, X. G. Gong, D. L. Feng, Tuning the band structure and superconductivity in single-layer FeSe by interface engineering. *Nat. Commun.* **5**, 5044 (2014).
22. J. Shiogai, Y. Ito, T. Mitsuhashi, T. Nojima, A. Tsukazaki, Electric-field-induced superconductivity in electrochemically etched ultrathin FeSe films on $SrTiO_3$ and MgO. *Nat. Phys.* **12**, 42–46 (2016).
23. Y. Sun, Y. Tsuchiya, T. Taen, T. Yamada, S. Pyon, A. Sugimoto, T. Ekino, Z. Shi, T. Tamegai, Dynamics and mechanism of oxygen annealing in $Fe_{1+y}Te_{0.6}Se_{0.4}$ single crystal. *Sci. Rep.* **4**, 4585 (2014).
24. G. M. Friederichs, M. P. B. Wörsching, D. Johrendt, Oxygen-annealing effects on superconductivity in polycrystalline $Fe_{1+x}Te_{1-y}Se_y$. *Supercond. Sci. Technol.* **28**, 095005 (2015).
25. T. J. Liu, X. Ke, B. Qian, J. Hu, D. Fobes, E. K. Vehstedt, H. Pham, J. H. Yang, M. H. Fang, L. Spinu, P. Schiffer, Y. Liu, Z. Q. Mao, Charge-carrier localization induced by excess Fe in the superconductor $Fe_{1+y}Te_{1-x}Se_x$. *Phys. Rev. B* **80**, 174509 (2009).
26. Y. Sun, T. Yamada, S. Pyon, and T. Tamegai, Influence of interstitial Fe to the phase diagram of $Fe_{1+y}Te_{1-x}Se_x$ single crystals. *Sci. Rep.* **6**, 32290 (2016).
27. J.-X. Yin, Z. Wu, X. Huang, J.-H. Wang, Z.-Y. Ye, R. Wu, X.-X. Wu, X.-J. Liang, H.-Q. Mao, J. Li, Y.-Y. Zhao, C.-S. Ting, J.-P. Hu, Z. Q. Wang, P.-H. Hor, H. Ding, S. H. Pan, Cooper pairing and phase coherence in iron superconductor Fe1+x(Te,Se). *ArXiv e-prints*, 1602.04961. (2016).
28. Y. Sun, T. Taen, T. Yamada, Y. Tsuchiya, S. Pyon, T. Tamegai, Evolution of superconducting and transport properties in annealed $FeTe_{1-x}Se_x$ ($0.1< x < 0.4$) multiband superconductors. *Supercond. Sci. Technol.* **28**, 044002 (2015).
29. A. Tamai, A. Y. Ganin, E. Rozbicki, J. Bacsa, W. Meevasana, P. D. C. King, M. Caffio, R. Schaub, S. Margadonna, K. Prassides, M. J. Rosseinsky, F. Baumberger, Strong electron correlations in the normal state of the iron-based $FeSe_{0.42}Te_{0.58}$ superconductor observed by angle-resolved photoemission spectroscopy. *Phys. Rev. Lett.* **104**, 097002 (2010).
30. H. Miao, P. Richard, Y. Tanaka, K. Nakayama, T. Qian, K. Umezawa, T. Sato, Y.-M. Xu, Y. B. Shi, N. Xu, X.-P. Wang, P. Zhang, H.-B. Yang, Z.-J. Xu, J. S. Wen, G.-D. Gu, X. Dai, J.-P. Hu, T. Takahashi, H. Ding, Isotropic superconducting gaps with enhanced pairing on electron Fermi surfaces in $FeTe_{0.55}Se_{0.45}$. *Phys. Rev. B* **85**, 094506 (2012).
31. J. Maletz, V. B. Zabolotnyy, D. V. Evtushinsky, S. Thirupathaiah, A. U. B. Wolter, L. Harnagea, A. N. Yaresko, A. N. Vasiliev, D. A. Chareev, A. E. Böhmer, F. Hardy, T. Wolf, C. Meingast, E. D. L. Rienks, B. Büchner, S. V. Borisenko, Unusual band renormalization in the simplest iron-based superconductor $FeSe_{1-x}$. *Phys. Rev. B* **89**, 220506 (2014).
32. Z. K. Liu, M. Yi, Y. Zhang, J. Hu, R. Yu, J.-X. Zhu, R.-H. He, Y. L. Chen, M. Hashimoto, R. G. Moore, S.-K. Mo, Z. Hussain, Q. Si, Z. Q. Mao, D. H. Lu, Z.-X. Shen, Experimental observation of incoherent-coherent crossover and orbital-dependent band renormalization in iron chalcogenide superconductors. *Phys. Rev. B* **92**, 235138 (2015).
33. F. Chen, B. Zhou, Y. Zhang, J. Wei,O. Hong-Wei, J.-F. Zhao, H. Cheng, Q.-Q. Ge, M. Arita, K. Shimada, H. Namatame, M. Taniguchi, Z.-Y. Lu, J. Hu, X.-Y. Cui, D. L. Feng, Electronic structure of $Fe_{1.04}Te_{0.66}Se_{0.34}$. *Phys. Rev. B* **81**, 014526 (2010).
34. J. Carlson, S. Reddy, Superfluid pairing gap in strong coupling. *Phys. Rev. Lett.* **100**, 150403 (2008).
35. M. Randeria, J.-M. Duan, L.-Y. Shieh, Bound states, Cooper pairing, and Bose condensation in two dimensions. *Phys. Rev. Lett.* **62**, 981–984 (1989).
36. B. Keimer, S. A. Kivelson, M. R. Norman, S. Uchida, J. Zaanen, From quantum matter to high-temperature superconductivity in copper oxides. *Nature* **518**, 179–186 (2015).
37. M. Randeria, Precursor pairing correlations and pseudogaps, in *High Temperature Superconductors, Proceedings of the International School of Physics "Enrico Fermi", Course CXXXVI*, J. R. Schrieffer G. Iadonisi, M. L. Chiafalo, Eds. (IOS Press, 1998), pp. 53–75.
38. M. R. Norman, A. Kanigel, M. Randeria, U. Chatterjee, J. C. Campuzano, Modeling the Fermi arc in underdoped cuprates. *Phys. Rev. B* **76**, 174501 (2007).
39. A. Schirotzek, Y.-i. Shin, C. H. Schunck, W. Ketterle, Determination of the superfluid gap in atomic Fermi gases by quasiparticle spectroscopy. *Phys. Rev. Lett.* **101**, 140403 (2008).

Acknowledgments

Funding: We acknowledge support from the United States–Israel Binational Science Foundation (grant 2014077). This work was supported, in part, by the Israel Science Foundation (grant 885/13). We thank the Helmholtz-Zentrum Berlin for the allocation of synchrotron radiation beamtime. We acknowledge SOLEIL for provision of synchrotron radiation facilities. The research leading to these results has received funding from the European Community's Seventh Framework Programme (FP7/2007-2013) under grant agreement no. 312284. M.R. was supported by NSF grant DMR-1410364. We thank the Aspen Center for Physics (supported by NSF grant PHY-1066293) for the hospitality during the writing of this paper. **Author contributions:** S.R., A.R., and A.K. performed the ARPES measurements with the help of E.D.L.R., A.T.-I., P.L.F., and F.B. K.B.C. performed the crystal growth. S.R. performed the transport measurements. S.R., M.R., and A.K. wrote the paper. M.R. and A.K. were responsible for the overall project planning and direction. **Competing interests:** The authors declare that they have no competing interests. **Data and materials availability:** All data needed to evaluate the conclusions in the paper are present in the paper and/or the Supplementary Materials. Additional data related to this paper may be requested from the authors at amitk@physics.technion.ac.il.

Submitted 26 September 2016
Accepted 24 February 2017
Published 21 April 2017
10.1126/sciadv.1602372

Citation: S. Rinott, K. B. Chashka, A. Ribak, E. D. L. Rienks, A. Taleb-Ibrahimi, P. Le Fevre, F. Bertran, M. Randeria, A. Kanigel, Tuning across the BCS-BEC crossover in the multiband superconductor $Fe_{1+y}Se_xTe_{1-x}$: An angle-resolved photoemission study. *Sci. Adv.* **3**, e1602372 (2017).